The role of friction in the yielding of adhesive non-Brownian suspensions

J. A. Richards, B. M. Guy, E. Blanco, M. Hermes, G. Poy, and W. C. K. Poon

Citation: Journal of Rheology **64**, 405 (2020); doi: 10.1122/1.5132395
View online: https://doi.org/10.1122/1.5132395
View Table of Contents: https://sor.scitation.org/toc/jor/64/2
Published by the The Society of Rheology

The role of friction in the yielding of adhesive non-Brownian suspensions

J. A. Richards,[1,a)] B. M. Guy,[1] E. Blanco,[1] M. Hermes,[1,2] G. Poy,[1,3] and W. C. K. Poon[1]

[1]*SUPA and School of Physics and Astronomy, The University of Edinburgh, Peter Guthrie Tait Road, Edinburgh, EH9 3FD, United Kingdom*
[2]*Debye Institute, Utrecht University, Princetonplein 5, 3584 CC Utrecht, The Netherlands*
[3]*Faculty of Mathematics and Physics, University of Ljubljana, Jadranska 19, 1000 Ljubljana, Slovenia*

(Received 17 October 2019; final revision received 7 January 2020; published 5 March 2020)

Abstract

Yielding behavior is well known in attractive colloidal suspensions. Adhesive non-Brownian suspensions, in which the interparticle bonds are due to finite-size contacts, also show yielding behavior. We use a combination of steady-state, oscillatory, and shear reversal rheology to probe the physical origins of yielding in the latter class of materials and find that yielding is not simply a matter of breaking adhesive bonds but involves unjamming from a shear-jammed state in which the microstructure has adapted to the direction of the applied load. Comparison with a recent constraint-based rheology model shows the importance of friction in determining the yield stress, suggesting novel ways to tune the flow of such suspensions. © *2020 The Society of Rheology.* https://doi.org/10.1122/1.5132395

I. INTRODUCTION

A recent paradigm shift in repulsive non-Brownian (nB) suspension rheology was inspired by the physics of jamming in dry grains. Shear thickening in such suspensions is now thought to be driven by the formation of compressive frictional contacts between neighboring particles beyond a certain critical, or onset, stress, σ^*, which overcomes the stabilizing interparticle repulsion [1,2]. Importantly, σ^* scales roughly as the inverse square of particle size [3] and is readily exceeded for nB suspensions, whose flow is, therefore, typically dominated by frictional contacts. Experiments [3,4] and simulations [5,6] are captured by a phenomenological model by Wyart and Cates (WC). In the WC model, a jamming volume fraction, at which the viscosity diverges, is set by a stress-dependent fraction of frictional contacts [7]; the WC model has then been successfully extended to time-dependent flows [8,9].

Non-Brownian suspensions occur widely in industrial products (concrete, paint, etc.) and their processing. The size of nB particles ($\gtrsim$10 μm) means that residual van der Waals attraction is all but inevitable despite steric or charge stabilization [3]. If strong enough, such an interaction gives rise to a yield stress, σ_y, below which suspensions cannot flow [10]. Such behavior occurs in, e.g., mine tailings and mineral slurries [11,12] or molten chocolate [13]. Controlling σ_y in suspensions is important for their stability during transport and shaping and for suspending various macroscopic particulates such as sand [14].

We have recently extended the WC framework to model the flow of nB suspensions with more varied particle-level interactions and, hence, to describe suspensions with a finite yield stress [15]. We treat interparticle friction as a constraint to relative sliding between particles that switches on with increasing stress. Adding a second constraint restricting interparticle rotation that is removed with increasing stress enables us to predict all classes of flow curves observed in the literature. A paradigmatic example of the second kind of constraint is adhesion: sticky finite-area contacts constraining interparticle rotation. Here the contact is pinned by a surface lengthscale, captured by, e.g., a modified–Johnson-Kendall-Roberts contact model [16], and the contact can only be broken if the applied stress exerts a critical torque on neighboring particles [17].

This "constraint rheology" of nB suspensions has a number of nontrivial implications, which are either discussed cursorily or remain implicit in our previous work [15]. Here, we present an extensive rheological study of a model adhesive nB suspension, cornstarch in oil, to highlight and discuss one such implication that yielding in adhesive nB suspensions should be qualitatively different from corresponding phenomena in Brownian (or colloidal) suspensions. In the latter, friction typically plays no role and the attraction between particles, which is described by a potential, does not by itself constrain interparticle rotation. There are similarities in the yielding phenomenology of the two kinds of systems. For example, we find that an adhesive nB suspension yields in two steps under certain rheological protocols, recalling attractive colloidal glasses [18]. However, such a resemblance turns out to be superficial and hides a profound difference in the underlying physical mechanisms.

Specifically, interparticle friction plays a key role in the genesis of a yield stress and in determining its magnitude. This role is unobvious in the form of the steady-state flow curve. However, the dependence of the steady-state yield stress, $\sigma_y^{(ss)}$, on the solid volume fraction, ϕ, points to a role for friction: $\sigma_y^{(ss)}(\phi)$ diverges before random close packing, ϕ_{rcp}, at a lower frictional jamming point, ϕ_μ. In contrast, large-amplitude oscillatory rheology returns a substantially

Note: This paper is part of the special issue on Physics of Dense Suspensions.
[a)]Author to whom correspondence should be addressed; electronic mail: jamesrichards92@gmail.com

lower yield stress, $\sigma_y^{(os)}$, which does diverge at ϕ_{rcp}. Finally, shear reversal experiments reveal that upon changing the direction of shear there is a transient yielding event at an intermediate "transient reversal yield stress," $\sigma_y^{(tr)} < \sigma_y^{(ss)}$. Interestingly, $\sigma_y^{(tr)}(\phi)$ follows the oscillatory yield stress at low ϕ, before increasing to approach the steady-state yield stress at higher ϕ.

Thus, the yield stress in adhesive nB suspensions is protocol dependent [19], which we connect with two fundamental features of nB suspensions. First, without thermal motion, sticky particles not already in contact will *not* encounter each other to build higher-order stress-bearing structures except under external deformation. So, second, given the low σ^* for nB particles, such deformation will almost always involve stress $>\sigma^*$, and so will bring interparticle friction into play. Therefore, adhesion seldom acts alone in nB suspensions. Using steady-state, oscillatory, and reversal rheology together allows us to illustrate these two features and highlight the differences between adhesive nB suspensions and colloidal suspensions with interparticle potential attraction.

II. CONSTRAINT RHEOLOGY

For later use, we first recast constraint rheology [15] for the specific case of a nB suspension with friction (constraining sliding) and adhesion (constraining rolling). Stripped to its bare essentials, WC proposes that increasing stress progressively makes frictional contacts, which pose additional constraints on interparticle motion by removing the freedom of contacting particles to slide past each other. In turn, this lowers the jamming volume fraction, causing shear thickening. Following WC's constraint-motivated train of thought, Guy *et al.* [15] propose that adhesion removes the freedom of contacting particles to roll on each other, thus lowering the jamming volume fraction; however, increasing stress progressively removes such constraints, thereby allowing the jamming volume fraction to rise, leading to shear thinning or even yielding from a shear-jammed state.

Specifically, following WC, the fraction of frictional contacts increases with stress, σ, according to

$$f(\sigma) = \exp\left[-\left(\frac{\sigma^*}{\sigma}\right)^{\beta}\right], \tag{1}$$

with β an exponent describing how rapidly f increases from 0 ($\sigma \ll \sigma^*$) to 1 ($\sigma \gg \sigma^*$). Additionally, stress decreases the fraction of adhesive constraints according to

$$a(\sigma) = 1 - \exp\left[-\left(\frac{\sigma_a}{\sigma}\right)^{\kappa}\right], \tag{2}$$

with σ_a setting the stress scale for breaking adhesive contacts and κ another exponent that captures how rapidly adhesive contacts are broken and the suspension shear thins. The jamming volume fraction is a function of these two variables, $\phi_J = \phi_J(f, a)$.

This function is well known in two limits. The maximum amorphous packing for frictionless, adhesionless hard spheres is random close packing, $\phi_J(f = 0, a = 0) \equiv \phi_{rcp} \approx 0.64$; the corresponding quantity for frictional hard spheres is $\phi_J(f = 1, a = 0) \equiv \phi_\mu \approx 0.55$ for highly frictional particles [20,21]. The limits with all-adhesive contacts are less well known. Simulating ballistic deposition [22,23] finds "adhesive loose packing" at $\phi_J(f = 1, a = 1) \equiv \phi_{alp} \approx 0.15$ and "adhesive close packing" at $\phi_J(f = 0, a = 1) \equiv \phi_{acp} \approx 0.51 = \phi_\mu$ given current levels of uncertainties, including likely protocol dependence.

Following WC, we interpolate to give

$$\begin{aligned}\phi_J(f, a) = af\phi_{alp} + a(1-f)\phi_{acp} + (1-a)f\phi_\mu \\ + (1-a)(1-f)\phi_{rcp}.\end{aligned} \tag{3}$$

For us, $\sigma^* \to 0$ and $f = 1$ always so that

$$\phi_J(f = 1, a) = a\phi_{alp} + (1-a)\phi_\mu. \tag{4}$$

Finally, as in WC, we take the relative viscosity to be

$$\eta_r = \left[1 - \frac{\phi}{\phi_J(a, f)}\right]^{-2}. \tag{5}$$

Together, Eqs. (2), (4), and (5) describe suspensions that yield and shear thin, class 1 flow curves in the terminology of [15].

To conclude this section, we make a proposal for terminology. In a canonical colloidal suspension, particles do not contact. Their interaction, described as the gradient of a potential, does *not* constrain interparticle rolling, which distinguishes it from the sticky contacts that concern us in this work. We propose to mark this important difference by strictly distinguishing between the terms "attraction" and "adhesion," with the latter denoting finite contact area with a concomitant rolling constraint. We find that markedly different physics underlies the yielding of adhesive nB suspensions and attractive suspensions [24,25].

III. EXPERIMENTAL SYSTEM AND METHODS

Cornstarch in aqueous media is a model for the rheology of purely repulsive nB suspensions, showing characteristic friction-driven shear thickening at a fixed onset stress [9,26]. When cornstarch is dispersed in nonaqueous solvents, shear thickening is no longer observed and a finite yield stress arises [27,28]. Adhesive particle interactions could originate from van der Waals forces, hydrogen bonding [29], or even capillary forces [30] from adsorbed water in cornstarch particles [31]. We disperse previously employed [9,26] cornstarch (Sigma Aldrich) in sunflower oil (Flora) to form a model adhesive nB suspension. The particles have a diameter of $d \approx 14\,\mu m$ and polydispersity of $\approx 40\%$ (from static light scattering [26]), and a density of $\rho_p = 1.45\,g\,cm^{-3}$. The sunflower oil has viscosity and density $\eta_f = 62\,mPa\,s$ and $\rho_f = 0.92\,g\,cm^{-3}$, respectively, at 20 °C. Cornstarch was dispersed by vortex mixing and stirring until visually homogeneous before roller mixing for $\gtrsim 2\,h$. Cornstarch does not swell in nonaqueous solvents [32] so that swelling corrections [31] are unnecessary.

We used a strain-controlled ARES-G2 rheometer for steady-state and oscillatory measurements and a controlled-torque DHR-2 rheometer for shear reversal experiments

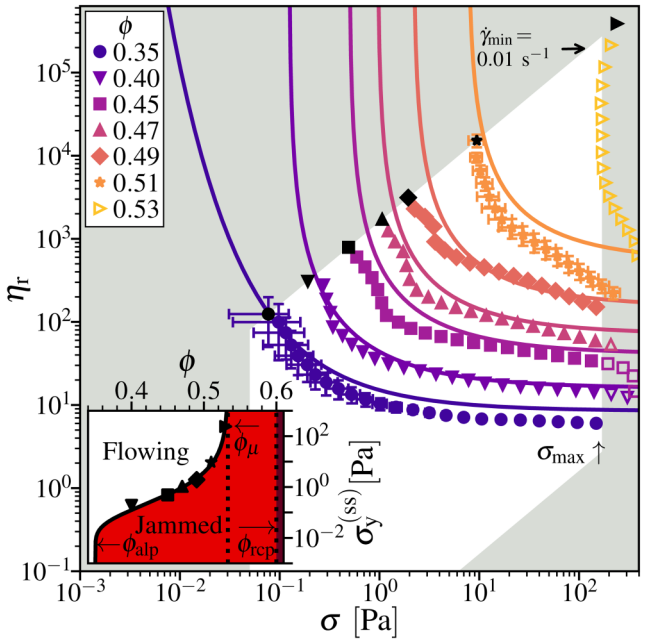

FIG. 1. Cornstarch-in-oil flow curves under imposed shear rate, $\dot{\gamma}$: relative viscosity, $\eta_r = \eta/\eta_f$, vs shear stress, σ. Unshaded, observable "window" (see text for details). See the legend for volume fractions, ϕ. Black points, $\sigma(\dot{\gamma}_{min}) \equiv \sigma_y^{(ss)}$; open symbols, unreliable measurements outside "window." Flow curves are averaged over three runs for $\phi \leq 0.47$ and two for $\phi = 0.51$ to estimate reliability; standard deviation shown when larger than marker. Lines, fit to constraint-based rheology model [15], Eqs. (2), (4), and (5), with $\phi_\mu = 0.533$, $\phi_{alp} = 0.35$, $\sigma_a = 0.2$ Pa, and $\kappa = 0.55$. Inset: steady-state yield stress, $\sigma_y^{(ss)}$, as a function of ϕ. Points, $\sigma_y^{(ss)}$, note that $\phi = 0.35$ is excluded as no yield stress is measured under imposed stress; solid line, yield stress from constraint-based model setting $\phi_J = \phi$. Shaded (red), jammed at steady state, $\phi_J < \phi$; unshaded, flowing at steady state, $\phi_J > \phi$; and dark (red) shaded, $\phi > \phi_{rcp} \sim 0.6$, dispersion not possible.

(both TA Instruments). Measurement geometry selection requires care. The 22 μm truncation gap of our cone-plate geometry was too small for our particles. In a Couette cell, sedimentation can give rise to an apparent yield stress [33], while stress variation across the gap can lead to spatial inhomogeneities [34]. We, therefore, used parallel plates (radius $R = 20$ mm, gap height $h = 1$ mm) with crosshatching (0.25 mm serrations) to reduce slip.

The steady-state rheology of our samples can be probed within a "window" of shear stresses and rates [Fig. 1 (unshaded region)]. The maximum stress in this window is set by sample fracture, which occurs for us at $\sigma_{max} \approx 180$ Pa [3]. The low shear rate limit, $\dot{\gamma}_{min}$, is set by the experimental time, which is limited by, e.g., drying or sedimentation of the sample, the latter setting a minimum stress at $\sigma_{min} = (\rho_p - \rho_f)gd \approx 0.05$ Pa, which is larger than the $\sigma_{min} \approx 0.01$ Pa set by the torque resolution of the ARES-G2. Finally, the maximum shear rate, $\dot{\gamma}_{max}$, is set by inertial sample rejection.

IV. THE STEADY-STATE YIELD STRESS

To measure flow curves, we presheared suspensions of various ϕ at $\dot{\gamma} = 10\,s^{-1}$ or $\dot{\gamma}(\sigma_{max})$, whichever is lower, and then dropped the imposed rate to $\dot{\gamma}_{min}$ to begin an up-sweep at 6 points per decade with a time interval of either 10 s or a longer interval to accumulate a strain of $\gamma = 10$. In a parallel-plate geometry, the imposed angular velocity, Ω, and the measured torque, M, give the rim shear rate, $\dot{\gamma} = \Omega R/h$, and the corrected stress, $\sigma = (M/2\pi R^3)(3 + d\ln M/d\ln\Omega)$ [35]. The relative viscosity, $\eta_r = \sigma/\dot{\gamma}\eta_f$, as a function of σ at different ϕ (Fig. 1) shows significant shear thinning at $\phi \gtrsim 0.35$: η_r decreases with σ to approach what appears to be a high-shear plateau, which, however, is obscured at higher ϕ by sample fracture at $\sigma_{max} \approx 180$ Pa. Similar flow curves have been widely reported in nB suspensions, including various 2–25 μm refractory particles and cocoa powder [11], 3–5 μm poly(methyl methacrylate) [36], and molten chocolate (≈15 μm sugar crystals suspended in a triglyceride) [13].

Such flow curves are typically taken to evidence interparticle attraction, whose strength is estimated by plotting $\sigma(\dot{\gamma})$ and extrapolating to $\dot{\gamma} = 0\,s^{-1}$ using an empirical model, e.g., Herschel–Bulkely or Casson, to obtain the steady-state yield stress, $\sigma_y^{(ss)}$. We estimate $\sigma_y^{(ss)}$ as the stress at the lowest accessed shear rate, i.e., $\sigma_y^{(ss)} = \sigma(\dot{\gamma}_{min} = 0.01\,s^{-1})$. For $\phi = 0.35$, this produced a finite $\sigma_y^{(ss)}$, but tests under controlled stress found that the sampled flowed at all applied stresses ($\sigma > 3$ mPa) so that in fact for $\phi = 0.35$ we take $\sigma_y^{(ss)} = 0$ Pa.

The role of friction in the yielding of our suspensions is revealed by the ϕ dependence of $\sigma_y^{(ss)}$ [Fig. 1 (inset)], which appears to diverge at $\phi \approx 0.54$. The frictionless and frictional jamming points of cornstarch in aqueous solvents are $\phi_{rcp} \approx 0.60$ [31] and $\phi_\mu \approx 0.50$, respectively. The latter is estimated from multiplying $\phi_{rcp} \approx 0.60$ by the measured weight-fraction ratio of 0.84 for random loose to random close packing for aqueous cornstarch [9]. We, therefore, take $\phi \approx 0.54$ at which $\sigma_y^{(ss)}(\phi) \to \infty$ to be the *frictional* jamming point, ϕ_μ, of cornstarch in oil. Consistent with this, we could make samples at $\phi > 0.54$; but these samples showed unsteady stick-slip flow or fracture, recalling similar behavior above ϕ_μ in aqueous cornstarch suspensions [26].

If our proposal that $\sigma_y^{(ss)} \to \infty$ at the frictional jamming point is correct, then the absence of shear thickening in our flow curves implies that our suspensions at $\phi < \phi_\mu$ always flow with frictional contacts after yielding ($f = 1$ because $\sigma^* \to 0$). Indeed, we find that Eqs. (2), (4), and (5) with $\phi_\mu = 0.533$, $\phi_{alp} = 0.35$, $\sigma_a = 0.2$ Pa, and $\kappa = 0.55$ can credibly account for both our flow curves [Fig. 1 (lines)] and $\sigma_y^{(ss)}(\phi)$ inferred from them (inset). Yielding in this suspension is then a matter of overcoming shear jamming due to a combination of adhesion and friction in the interval $\phi_{alp} < \phi < \phi_\mu$. This contrasts with colloidal systems, where a gelled state can form without external perturbation due to thermal motion, whereas in a nB system structure can only form under external mechanical perturbation such as shear. Unjamming this shear-jammed state requires breaking adhesive bonds with stress, removing constraints progressively until ϕ_J exceeds the sample ϕ at some critical stress that we identify as $\sigma_y^{(ss)}$. This yield stress first arises at the minimum jamming volume fraction of $\phi_J(a = 1, f = 1) = \phi_{alp}$ and diverges at the maximum value of $\phi_J = \phi_\mu$.

Our $\phi_{alp} = 0.35$ is considerably higher than ≈ 0.15 found in recent simulations [22,23]. This may partly reflect particle properties (monodisperse spheres vs polydisperse cornstarch

grains), but it may also reflect fundamental physics. If the solidlike state at $\sigma < \sigma_y^{(ss)}$ is due to jamming, then its properties could depend on how jamming was induced in the first place. As ballistic deposition [22,23] and steady shear give different jammed states, the rigidity percolation threshold, ϕ_{alp}, may also differ.

Since our particle contacts are sticky, frictional, and of finite area, they form rigid bonds so that contact and rigidity percolation coincide, and the value of ϕ_{alp} should represent this coincident percolation threshold under shear. Indeed, our ϕ_{alp} is similar to the percolation threshold found for frictionless and adhesionless nB suspensions (of monodisperse spheres) under shear [37], which furthermore is not strongly affected by the presence of additional constraints such as friction [38]. In contrast, for attractive interactions without bond rigidity, percolation and rigidity percolation differ [39].

V. THE OSCILLATORY YIELD STRESS

To disentangle the entwined roles of friction and adhesion in steady-state flow, we performed oscillatory rheology. Applying sinusoidal shear at an (angular) frequency of $\omega = 10$ rad s^{-1}, we measured the storage and loss moduli, G' and G'', in a downsweep of strain amplitude, γ_0, starting from either $\gamma_0 = 10$ or the highest strain amplitude reachable without fracture; this removed loading effects and ensured repeatability. The measured $G'(\gamma_0)$ and $G''(\gamma_0)$ at $\phi = 0.51$ [Fig. 2(a) (inset)] show a slow decrease with γ_0 but no sudden yielding. The main figure replots these data against the so-called "elastic stress" [40], $\sigma' = G'\gamma_0$. If G' was frequency independent and G'' scaled viscously ($\propto\omega$), σ' would represent the stress at zero frequency. In this representation, it is clear that the sample yields—the moduli drop abruptly—at some critical stress. This is confirmed by plotting $\gamma_0(\sigma')$, an approximate static (i.e., $\dot\gamma$ or $\omega \to 0$) stress-strain curve [Fig. 2(b)]. This function is ω-independent up to an oscillatory yield stress, $\sigma_y^{(os)} \approx 0.03$ Pa, where γ_0 makes an abrupt jump by more than 3 orders of magnitude over a very small interval of σ'.

In the raw data, we find G' is smaller than G'' for all γ_0 at $\omega = 10$ rad s^{-1}. This is simply because $G'' \sim \eta\omega$ while G' is essentially η-independent, and we have used a high-viscosity solvent to bring the relevant phenomena into the stress window of our rheometer. At the lower frequency of $\omega = 1$ rad s^{-1}, we indeed recover $G' > G''$ at small strains, as expected for a "solidlike" sample.

The dependence of the oscillatory yield stress on suspension concentration, $\sigma_y^{(os)}(\phi)$, is shown in Fig. 3, where we have also replotted the corresponding function for the steady-state yield stress, $\sigma_y^{(ss)}(\phi)$, for comparison. Two features immediately stand out. First, $\sigma_y^{(os)} \ll \sigma_y^{(ss)}$, by 1.5 orders of magnitude at $\phi = 0.4$ and rising to 4 orders of magnitude at $\phi \lesssim 0.53$. Second, we can measure a finite $\sigma_y^{(os)}$ considerably beyond $\phi_\mu \approx 0.53$. Indeed, fitting to $A(1-\phi/\phi_c)^{-l}$ shows that $\sigma_y^{(os)}(\phi)$ diverges (with $A = 5\times10^{-4}$ and $l = 2.2$) at $\phi_c \approx 0.603$, which is ϕ_{rcp} for aqueous cornstarch.

These features suggest that oscillatory shear removes frictional contacts to enable probing of yielding to a frictionless state, which therefore does not jam until ϕ_{rcp}. The oscillatory shear applied is sufficient to break and mobilize adhesive bonds. What we observe can, therefore, be usefully compared with the way repeated oscillatory shear removes or relaxes contacts in nonadhesive nB systems [41,42], and with shaking dry grains to compactify the packing from (frictional) random loose packing to (frictionless) random close packing [43]. The magnitude of $\sigma_y^{(os)}$, therefore, reflects the adhesive contact strength alone without the effects of friction. However, $\sigma_y^{(os)}$ does not directly measure the adhesive bond strength, $\sigma_a = 0.2$ Pa, that we have previously extracted from

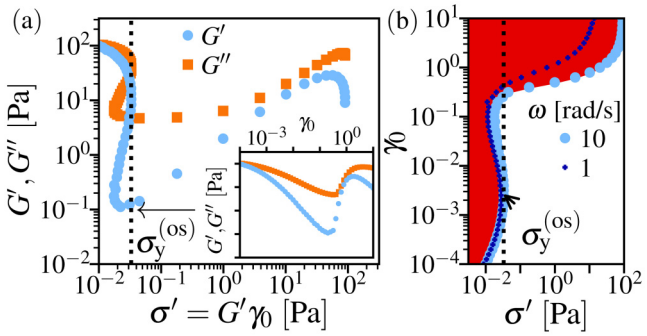

FIG. 2. Oscillatory rheology at $\phi = 0.51$, for a decreasing imposed strain amplitude, γ_0. (a) Elastic modulus, G' (light blue circle), and loss modulus, G'' (orange square), as a function of elastic stress, $\sigma' = G'\gamma_0$. Data are taken at 10 points per decade from $\gamma_0 = 10$ to $\gamma_0 = 10^{-4}$ at an (angular) frequency $\omega = 10$ rad s^{-1} with one delay cycle and seven measurement cycles. Inset: moduli vs γ_0. (b) Load curve: strain amplitude, γ_0, vs elastic stress, σ', at $\omega = 1$ rad s^{-1} (dark blue cross) taken with one delay cycle and one measurement cycle and 10 rad s^{-1} (light blue circle), as in (a). The oscillatory yield stress, $\sigma_y^{(os)}$ (dotted line), is identified from the value of σ', where $d\sigma'/d\gamma_0 = 0$ with the minimum γ_0 at $\omega = 10$ rad s^{-1}. The oscillatory yield stress is also indicated in (a) for comparison. Shaded (red), predicted jammed region and unshaded, predicted (transient) flow region.

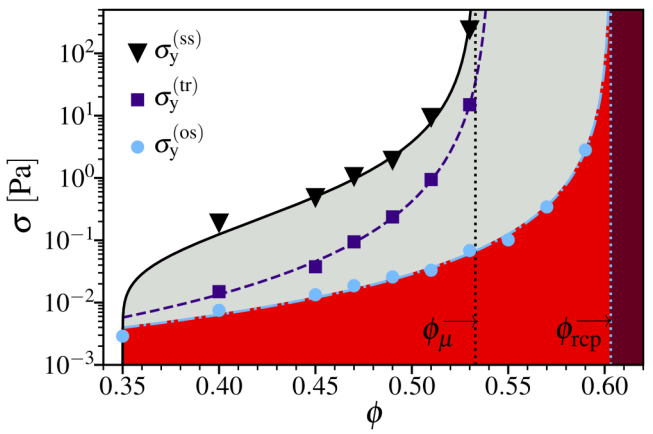

FIG. 3. ϕ dependence of yield stresses. Symbols: ▼, steady-state yield stress, $\sigma_y^{(ss)}$; ■, transient yield stress upon shear reversal, $\sigma_y^{(tr)}$; and •, oscillatory yield stress, $\sigma_y^{(os)}$. Lines: solid black, yield stress of constraint-based model, parameters as in Fig. 1; dashed purple, fit of $\sigma_y^{(tr)}$ to $A(1-\phi/\phi_{crit})^{-l}$, with $\phi_{crit} = 0.541 \pm 0.002$ ($A = 3\times10^{-4}$ and $l = 2.8$); dot-dashed light blue, fit of $\sigma_y^{(os)}$ to $A(1-\phi/\phi_{rcp})^{-l}$ to extract $\phi_{rcp} = 0.603 \pm 0.003$ ($A = 5\times10^{-4}$ and $l = 2.2$); black dotted, $\phi_\mu = 0.533$ from constraint-based model; and light blue dotted, ϕ_{rcp} from $\sigma_y^{(os)}$ divergence. Shaded regions: unshaded, continuous flow; light (gray) shading, jammed at steady state but transient flow possible [$\sigma_y^{(os)}(\phi) < \sigma < \sigma_y^{(ss)}(\phi)$], indicating range of possible protocol-dependent yield-stress measurements; (red) shading, jammed at steady-state and no transient flow and dark (red) shading, no dispersion possible ($\phi > \phi_{rcp}$).

the steady-state flow curves, because $\sigma_y^{(os)}$ is a collective property reflecting σ_a and suspension structure.

After the abrupt rise in $\gamma_0(\sigma')$ at $\sigma_y^{(os)}$ [Fig. 2(b)] the function bends over at $\gamma_0 \approx 0.5$, whereupon σ' rises rapidly with γ_0. This suggests that the system rejams with strain after yielding at $\sigma_y^{(os)}$ so that yielding at $\sigma_y^{(os)}$ is only transient. We attribute the rejamming to the remaking of frictional contacts, which occurs at a strain where frictional contacts have been found to reform after reversal in shear-thickening nB suspensions at a similar volume fraction relative to ϕ_{rcp} [44]. However, because we impose a finite-amplitude sinusoidal strain, we cannot access true jamming ($\dot{\gamma} = 0$) and can only infer it in a manner analogous to inferring jamming in shear-thickening nB suspensions under imposed shear rate [6]. Moreover, our data at $\sigma > \sigma_y^{(os)}$ is strongly frequency dependent [Fig. 2(b)], with σ' shifting linearly with ω, indicating viscous behavior. Thus, the second upturn in $\gamma_0(\sigma')$ at large σ' should *not* be directly interpreted as a second yielding event.

VI. THE TRANSIENT REVERSAL YIELD STRESS

A protocol that does show transient yielding, rejamming, and a second, permanent yielding is shear reversal. It has been used to reveal the role of friction in repulsive nB suspensions [44,45]: abruptly reversing the shear direction during steady-state shear breaks all frictional contacts, which are only reformed when a reversed strain of order unity has been accumulated.

To reach a well-defined initial state, samples were presheared just below the fracture stress, σ_{max}, for 100 s, left quiescent for 100 s, and then stressed at a constant $\sigma < \sigma_{max}$ for 1000 s in the opposite direction. We work in terms of the rim strain, γ, and apparent stress, $\sigma = 3M/2\pi R^3$, correct at yielding, where $d\ln M/d\ln\Omega = 0$. The time-dependent strain response in the new direction, $\gamma_{rev}(t)$, was measured over a range of stresses. Data for $\phi = 0.51$ [Fig. 4(a)] are typical.

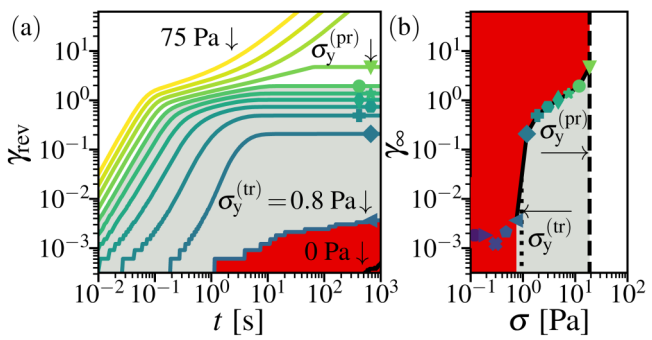

FIG. 4. Shear reversal at $\phi = 0.51$. (a) Time-dependent strain response after application of stress in the reverse direction, $\gamma_{rev}(t)$, for imposed stresses, σ, spaced logarithmically at 5 points per decade from 0.075 Pa (data shown from 0.8 Pa) to 75 Pa [dark (teal) to light (yellow)] and 0 Pa (black). Stress given by symbol (and color) in (b) for states that are jammed at $t = 1000$ Pa; for flowing states $\sigma = 30$, 47 and 75 Pa. Response types: (red) shaded, range of responses showing creep ($\sigma < \sigma_y^{(tr)}$); light (gray) shaded, transient yielding response ($\sigma_y^{(tr)} < \sigma < \sigma_y^{(pr)}$); and unshaded, permanently flowing ($\sigma > \sigma_y^{(pr)}$). (b) Long-time limiting strain, $\gamma_\infty(\sigma) \equiv \gamma_{rev}(t = 10^3\,s)$ vs σ (symbols). Dotted line, $\sigma_y^{(tr)}$, indicates the stress for transient yielding, identified from the largest increase in $\log(\gamma_\infty)$ with $\log(\sigma)$; dashed line indicates, $\sigma_y^{(pr)}$, the stress to permanently flow. Shading: unshaded, flowing states; light (gray) shaded, transiently flowing states (will jam at γ_∞); and, (red) shaded, inaccessible jammed states.

At $\sigma < 0.8$ Pa, we find a sublinear growth of $\gamma_{rev}(t)$, or creep; its occurrence at $\sigma = 0$ Pa shows that creep is a remnant of preshear. Above the transient reversal yield stress $\sigma_y^{(tr)} = 0.8$ Pa, the suspension transiently unjams and flows at constant acceleration, $\gamma_{rev} \propto t^2$, which reflects instrument inertia. Below $\sigma = 20$ Pa, the flowing suspension then rejams at $\gamma_{rev} \approx O(1)$. This strain is not recoverable. Above a permanent reversal yield stress $\sigma_y^{(pr)} = 20$ Pa, the suspension unjams again, now permanently yielding to continuous, viscous flow with $\gamma_{rev} \propto t$.

Figure 4(b) shows the long-time limiting strain, γ_∞, for $\sigma < 20$ Pa as a function of σ. (Continuous flow at higher σ means $\gamma_\infty \to \infty$.) The two-stepped form of $\gamma_\infty(\sigma)$ recalls $\gamma_0(\sigma')$ measured using the oscillatory protocol [Fig. 2(b)]. Now, however, all states in γ_∞ are jammed, with well-defined plateaus in $\gamma_{rev}(t)$ up to $\gamma_\infty \approx \mathcal{O}(1)$ so that the second upturn in $\gamma_\infty(\sigma)$ at $\sigma_y^{(pr)}$ indeed evidences a second yield stress. We compare the value of this yield stress with the steady-state yield stress, $\sigma_y^{(ss)}$, at a range of concentrations in Fig. 5. Across ϕ, they are comparable to within experimental uncertainties (Fig. 5).

An exception occurs at $\phi = 0.51$, where $\sigma_y^{(pr)}$ corresponds more closely to the peak stress measured at $\dot{\gamma}_{min}$ after preshear [Fig. 5 (black symbol)]. This peak may be indicative of banding [46], suggesting that the suspension may yield into a banded state above $\sigma_y^{(pr)}$. This single discrepancy does not impact our conclusion that $\sigma_y^{(ss)}$ and $\sigma_y^{(pr)}$ are comparable, and both diverge at ϕ_μ. This agreement is unsurprising: above $\sigma_y^{(pr)}$, the system flows continuously under the reversed applied stress and a frictional contact network is fully formed ($f = 1$) so that $\sigma_y^{(pr)}$ reflects both friction and adhesion.

More interestingly, the dependence on concentration of the lower, transient reversal yield stress, $\sigma_y^{(tr)}(\phi)$, is intermediate between that of $\sigma_y^{(os)}(\phi)$ and $\sigma_y^{(ss)}(\phi)$. Fitting to $A(1-\phi/\phi_c)^{-l}$ gives a curve (with $A = 3\times10^{-4}$ and $l = 2.8$) that approaches $\sigma_y^{(os)}(\phi)$ from above at low ϕ and approaches $\sigma_y^{(ss)}(\phi)$ from

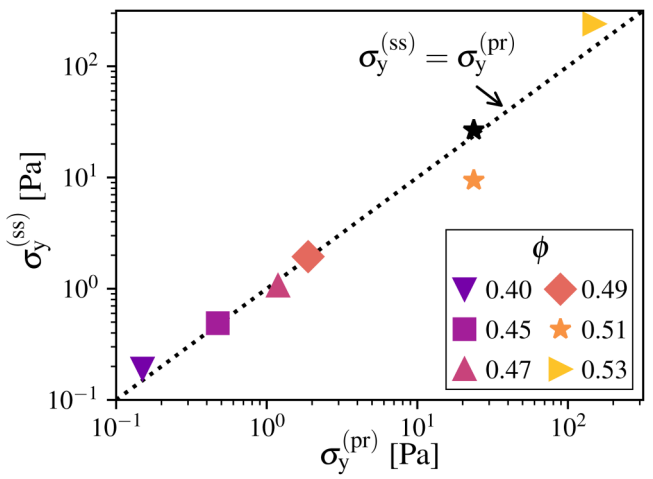

FIG. 5. Comparison of the steady-state yield stress, $\sigma_y^{(ss)}$ (colored), and the permanent reversal yield stress, $\sigma_y^{(pr)}$ at different volume fractions (see the legend). The dashed line has unit slope. For $\phi = 0.51$ a measurement of the peak stress measured at $\dot{\gamma}_{min}$ after preshear is also shown (black star); these measurements do not differ at other ϕ.

below at high ϕ, diverging at $\phi_c = 0.541 \pm 0.002$, which is the same as ϕ_μ inferred from $\sigma_y^{(ss)}(\phi)$ to within experimental uncertainties.

The behavior of $\sigma_y^{(tr)}$ can be understood using ideas originally invoked to explain the "fragility" of shear-jammed states in repulsive nB suspensions [47] (Fig. 6). Consider first the suspension structure during preshear. The high applied stress ($\sigma \gg \sigma_a$) breaks all-adhesive contacts, and the microstructure resembles that of a purely frictional nB suspension at the same ϕ, where at a high enough ϕ, sample-spanning force chains develop in the compressive direction [filled black circles in Fig. 6(a) (top)] in which particles form frictional contacts [highlighted with (red) tangential lines in Fig. 6(a)] [6]. Simulations of hard spheres find such contact percolation at $0.3 \lesssim \phi \lesssim 0.4$ [37], irrespective of the presence or absence of friction [38]. These force chains, however, do not lead to shear jamming because as they buckle under applied stress the suspension is not dense enough for other, stabilizing frictional contacts to form.

Such reinforcement becomes possible as $\phi \to \phi_\mu$, giving rise to "supporting" frictional force chains [filled gray circles in Fig. 6(b) (top)] [6], which leads to shear jamming at ϕ_μ in purely frictional nB suspensions [48]. In a frictional nB suspension, the compressional force chains are broken upon reversal, and the supporting force chains are not well-aligned enough to the new compression direction to cause shear jamming immediately upon reversal. Frictional nB suspensions are, therefore, "fragile"—they are only jammed (solid like) relative to a particular driving stress component.

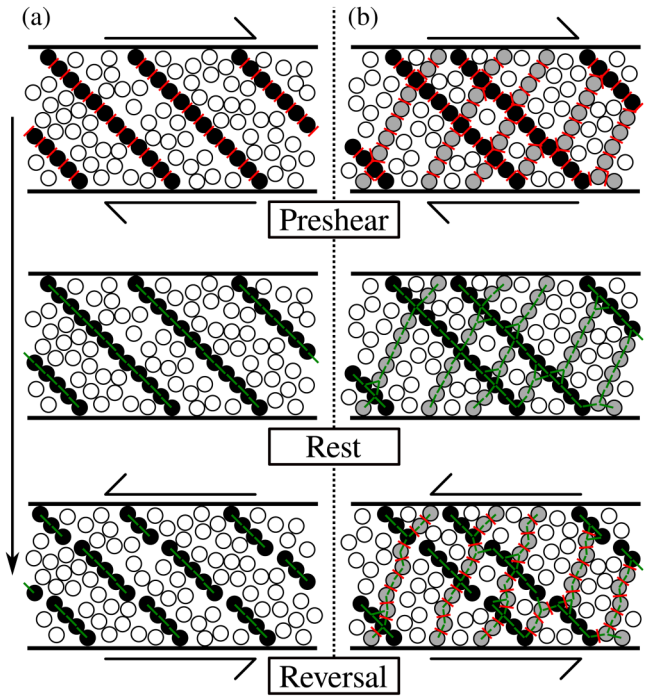

FIG. 6. Schematic illustration of fragility in adhesive nB suspensions under shear reversal (after Cates *et al.* [47]). (a) Microstructure and particle interactions for moderate volume fractions, $\phi_{alp} < \phi \ll \phi_\mu$, during: high-stress preshear (top), rest (middle), and shear reversal (bottom). Half-headed arrows indicate the direction of the applied shear stress, vertical arrow order of steps in protocol. Particles: filled black, in "force chains" during preshear; white filled, spectator particles. Tangential (red) lines show compressive frictional contacts, and center-to-center (green) lines show adhesive contacts. (b) Corresponding microstructure and particle interactions at a high volume fraction $\phi \lesssim \phi_\mu$. Filled gray particles in supporting contact network during preshear.

Upon the cessation of preshear in an adhesive suspension, all the contacts become adhesive as $\sigma \ll \sigma_a$ [highlighted with center-to-center (green) lines in Figs. 6(a) (middle) and 6(b) (middle)]. Consider what happens when shear is applied in the reverse direction. Now, even at ϕ significantly below ϕ_μ, system-spanning adhesive chains exist that can bear finite tensile stress. These are the sole load-bearing structures at low volume fractions [Fig. 6(a) (bottom)]. Yielding at $\sigma_y^{(tr)}$, therefore, involves breaking tensile, rather than compressive, contacts so that friction is not important, and $\sigma_y^{(tr)} \approx \sigma_y^{(os)}$. As $\phi \to \phi_\mu$, however, frictional force chains come into being immediately upon reversal [Fig. 6(b) (bottom)], these being originally created as "supporting" frictional force chains during preshear. Although not entirely aligned with the new compressive direction, the presence of adhesion can stabilize them to a near-compressive load, similar to the argument for particles of finite softness [47]. To yield transiently upon reversal, these compressive force chains must be buckled. Now, yielding involves both friction and adhesion so that $\sigma_y^{(tr)}(\phi)$ increases as $\phi \to \phi_\mu$.

VII. CONCLUSION

All salient aspects of our findings can be inferred from Fig. 3. Under continuous flow, our suspensions display a steady-state yield stress, $\sigma_y^{(ss)}$, which emerges at $\phi_{alp} \approx 0.35$ and diverges at the frictional jamming point, $\phi_\mu \approx 0.54$. Both critical concentrations testify to the role of friction. In contrast, oscillatory rheology reveals adhesion acting alone. The oscillatory yield stress, $\sigma_y^{(os)}$, diverges at the frictionless jamming point, $\phi_{rcp} \approx 0.60$, and $\sigma_y^{(os)}(\phi) \ll \sigma_y^{(ss)}(\phi)$, recalling the compaction of dry grains by tapping. Finally, transient yielding under shear reversal occurs at an intermediate stress, $\sigma_y^{(tr)}$. It is initially close to (yet slightly above) $\sigma_y^{(os)}$ but increases at higher ϕ to approach $\sigma_y^{(ss)}$ and diverge at ϕ_μ.

Our results raise a number of issues for future exploration. If our microstructural proposals inspired by the notion of fragility first invoked to explain the rheology of repulsive nB suspensions are essentially correct, then a formal extension of the fragility concept to adhesive nB suspensions should prove fruitful. Figure 3 suggests that $\sigma_y^{(os)}$ and $\sigma_y^{(ss)}$ are the lower and upper bound for the yield stress of an adhesive nB suspension, because the former probes adhesion alone, while the latter probes a maximally coupled adhesive-frictional state. Systematic investigation of other protocols besides shear reversal should test this suggestion. When combined with simulations, the results will give a more detailed understanding of the protocol-dependent yielding of such suspensions.

Throughout, we have commented on the difference between attractive and adhesive systems. Potential attraction does not constrain interparticle motion and cannot stabilize compressive force chains. It, therefore, does not interact with friction in the ways that we have invoked to discuss adhesive nB suspensions. Indeed, it has been proposed [10] and simulations suggest that yielding in attractive systems is distinct from shear jamming, with the yield stress arising from an isotropic state and simply masking shear thickening [25,49].

TABLE I. List of symbols beyond standard rheometric symbols.

Symbol	Definition
a	Proportion of adhesive contacts in the model of Guy *et al.* [15]
f	Proportion of frictional contacts in the WC model [7]
σ_a	Strength of adhesive contact
σ^*	Onset stress for frictional contacts
ϕ_J	Jamming volume fraction where $\eta_r \to \infty$ as $\phi \to \phi_J$
ϕ_{rcp}	Random close packing, jamming point for frictionless and adhesionless particles
ϕ_μ	Jamming point for frictional but adhesionless particles
ϕ_{acp}	Adhesive close packing, jamming point for frictionless but adhesive particles
ϕ_{alp}	Adhesive loose packing, jamming point for frictional and adhesive particles
γ_{rev}	Time-dependent strain upon application of a reverse stress, the opposite direction to preshear
γ_∞	Long-time-limit reversal strain, $\gamma_{rev}(t = 10^3\ s)$, for nonflowing states
σ'	Elastic stress in phase with applied deformation, $\sigma' = G'\gamma_0$
σ_{max}	Fracture stress for parallel-plate rheometry
$\sigma_y^{(ss)}$	Steady-state yield stress from the minimum shear rate accessed on the flow curve
$\sigma_y^{(os)}$	Oscillatory yield stress defined from the peak elastic stress
$\sigma_y^{(tr)}$	Stress to transiently yield upon reversal, from the largest increase in $\log \gamma_\infty$ with $\log \sigma$
$\sigma_y^{(pr)}$	Stress to permanently yield upon reversal to a flowing state $\gamma_{rev} \propto t$

A systematic comparison between the two kinds of suspensions remains to be done.

Our finding that $\sigma_y^{(os)} \ll \sigma_y^{(ss)}$ suggests that the best way to lower the latter dramatically is not to perturb the interparticle adhesion (e.g., through surface "stabilizers") but to diminish or eliminate interparticle friction. As in purely frictional nB suspensions, applying orthogonal shear or acoustic perturbations [44], which mimics our oscillatory protocol, may accomplish this goal. Alternatively, one may increase σ^* (which is ≈ 0 in our case) until $\sigma^* > \sigma_a$. Our results suggest, and the constraint rheology model predicts, that this should lead to a drop in σ_y by many orders of magnitude, because yielding will no longer be dominated by friction. This insight generates a new "design principle" for surfactants as yield stress modifiers in adhesive nB suspensions, seeing these molecules as lubricants rather than stabilizers.

VIII. LIST OF SYMBOLS

All symbols used throughout and not defined in the Official symbols and nomenclature of The Society of Rheology are listed in Table I.

ACKNOWLEDGMENTS

This work was supported by the UK Engineering and Physical Sciences Research Council (EPSRC, Nos. EP/N025318/1 and EP/L015536/1); J.A.R. was funded by the EPSRC Centre for Doctoral Training in Soft Matter and Functional Interfaces (SOFI CDT) and AkzoNobel and E.B. by Mars Chocolate UK Ltd. Data relevant to this work can be accessed on Edinburgh DataShare at https://doi.org/10.7488/ds/2634.

REFERENCES

[1] Comtet, J., G. Chatté, A. Niguès, L. Bocquet, A. Siria, and A. Colin, "Pairwise frictional profile between particles determines discontinuous shear thickening transition in non-colloidal suspensions," Nat. Commun. **8**, 15633 (2017).

[2] Clavaud, C., A. Bérut, B. Metzger, and Y. Forterre, "Revealing the frictional transition in shear-thickening suspensions," Proc. Natl. Acad. Sci. U.S.A. **114**, 5147–5152 (2017).

[3] Guy, B. M., M. Hermes, and W. C. K. Poon, "Towards a unified description of the rheology of hard-particle suspensions," Phys. Rev. Lett. **115**, 088304 (2015).

[4] Royer, J. R., D. L. Blair, and S. D. Hudson, "Rheological signature of frictional interactions in shear thickening suspensions," Phys. Rev. Lett. **116**, 188301 (2016).

[5] Seto, R., R. Mari, J. F. Morris, and M. M. Denn, "Discontinuous shear thickening of frictional hard-sphere suspensions," Phys. Rev. Lett. **111**, 218301 (2013).

[6] Mari, R., R. Seto, J. F. Morris, and M. M. Denn, "Shear thickening, frictionless and frictional rheologies in non-Brownian suspensions," J. Rheol. **58**, 1693–1724 (2014).

[7] Wyart, M., and M. E. Cates, "Discontinuous shear thickening without inertia in dense non-Brownian suspensions," Phys. Rev. Lett. **112**, 098302 (2014).

[8] Chacko, R. N., R. Mari, M. E. Cates, and S. M. Fielding, "Dynamic vorticity banding in discontinuously shear thickening suspensions," Phys. Rev. Lett. **121**, 108003 (2018).

[9] Richards, J. A., J. R. Royer, B. Liebchen, B. M. Guy, and W. C. K. Poon, "Competing timescales lead to oscillations in shear-thickening suspensions," Phys. Rev. Lett. **123**, 038004 (2019).

[10] Brown, E., N. A. Forman, C. S. Orellana, H. Zhang, B. W. Maynor, D. E. Betts, J. M. DeSimone, and H. M. Jaeger, "Generality of shear thickening in dense suspensions," Nat. Mater. **9**, 220–224 (2010).

[11] Zhou, J. Z. Q., P. H. T. Uhlherr, and F. T. Luo, "Yield stress and maximum packing fraction of concentrated suspensions," Rheol. Acta **34**, 544–561 (1995).

[12] Nguyen, Q., and D. Boger, "Application of rheology to solving tailings disposal problems," Int. J. Mineral Process. **54**, 217–233 (1998).

[13] Blanco, E., D. J. M. Hodgson, M. Hermes, R. Besseling, G. L. Hunter, P. M. Chaikin, M. E. Cates, I. Van Damme, and W. C. K. Poon, "Conching chocolate is a prototypical transition from frictionally jammed solid to flowable suspension with maximal solid content," Proc. Natl. Acad. Sci. U.S.A. **116**, 10303–10308 (2019).

[14] Ovarlez, G., F. Mahaut, S. Deboeuf, N. Lenoir, S. Hormozi, and X. Chateau, "Flows of suspensions of particles in yield stress fluids," J. Rheol. **59**, 1449–1486 (2015).

[15] Guy, B. M., J. A. Richards, D. J. M. Hodgson, E. Blanco, and W. C. K. Poon, "Constraint-based approach to granular dispersion rheology," Phys. Rev. Lett. **121**, 128001 (2018).

[16] Heim, L.-O., J. Blum, M. Preuss, and H.-J. Butt, "Adhesion and friction forces between spherical micrometer-sized particles," Phys. Rev. Lett. **83**, 3328–3331 (1999).

[17] Pantina, J. P., and E. M. Furst, "Elasticity and critical bending moment of model colloidal aggregates," Phys. Rev. Lett. **94**, 138301 (2005).

[18] Pham, K. N., G. Petekidis, D. Vlassopoulos, S. U. Egelhaaf, P. N. Pusey, and W. C. K. Poon, "Yielding of colloidal glasses," Europhys. Lett. **75**, 624–630 (2006).

[19] Nguyen, Q. D., T. Akroyd, D. C. De Kee, and L. Zhu, "Yield stress measurements in suspensions: An inter-laboratory study," Korea Aust. Rheol. J. **18**, 15–24 (2006).

[20] Jerkins, M., M. Schröter, H. L. Swinney, T. J. Senden, M. Saadatfar, and T. Aste, "Onset of mechanical stability in random packings of frictional spheres," Phys. Rev. Lett. **101**, 018301 (2008).

[21] Silbert, L. E., "Jamming of frictional spheres and random loose packing," Soft Matter **6**, 2918–2924 (2010).

[22] Liu, W., S. Li, A. Baule, and H. A. Makse, "Adhesive loose packings of small dry particles," Soft Matter **11**, 6492–6498 (2015).

[23] Liu, W., Y. Jin, S. Chen, H. A. Makse, and S. Li, "Equation of state for random sphere packings with arbitrary adhesion and friction," Soft Matter **13**, 421–427 (2017).

[24] Pednekar, S., J. Chun, and J. F. Morris, "Simulation of shear thickening in attractive colloidal suspensions," Soft Matter **13**, 1773–1779 (2017).

[25] Singh, A., S. Pednekar, J. Chun, M. M. Denn, and J. F. Morris, "From yielding to shear jamming in a cohesive frictional suspension," Phys. Rev. Lett. **122**, 098004 (2019).

[26] Hermes, M., B. M. Guy, W. C. K. Poon, G. Poy, M. E. Cates, and M. Wyart, "Unsteady flow and particle migration in dense, non-Brownian suspensions," J. Rheol. **60**, 905–916 (2016).

[27] Freundlich, H., and H. L. Röder, "Dilatancy and its relation to thixotropy," Trans. Faraday Soc. **34**, 308–316 (1938).

[28] Gálvez, L. O., S. de Beer, D. van der Meer, and A. Pons, "Dramatic effect of fluid chemistry on cornstarch suspensions: Linking particle interactions to macroscopic rheology," Phys. Rev. E **95**, 030602 (2017).

[29] James, N. M., C.-P. Hsu, N. D. Spencer, H. M. Jaeger, and L. Isa, "Tuning interparticle hydrogen bonding in shear-jamming suspensions: Kinetic effects and consequences for tribology and rheology," J. Phys. Chem. Lett. **10**, 1663–1668 (2019).

[30] Koos, E., and N. Willenbacher, "Capillary forces in suspension rheology," Science **331**, 897–900 (2011).

[31] Han, E., N. Van Ha, and H. M. Jaeger, "Measuring the porosity and compressibility of liquid-suspended porous particles using ultrasound," Soft Matter **13**, 3506–3513 (2017).

[32] Chen, D. Z., H. Zheng, D. Wang, and R. P. Behringer, "Discontinuous rate-stiffening in a granular composite modeled after cornstarch and water," Nat. Commun. **10**, 1283 (2019).

[33] Fall, A., F. Bertrand, G. Ovarlez, and D. Bonn, "Yield stress and shear banding in granular suspensions," Phys. Rev. Lett. **103**, 178301 (2009).

[34] Fall, A., A. Lemaître, F. Bertrand, D. Bonn, and G. Ovarlez, "Shear thickening and migration in granular suspensions," Phys. Rev. Lett. **105**, 268303 (2010).

[35] Macosko, C. W., *Rheology: Principles, Measurements, and Applications*, Advances in Interfacial Engineering (VCH, New York, 1993).

[36] Heymann, L., S. Peukert, and N. Aksel, "On the solid-liquid transition of concentrated suspensions in transient shear flow," Rheol. Acta **41**, 307–315 (2002).

[37] Gallier, S., E. Lemaire, F. Peters, and L. Lobry, "Percolation in suspensions and de Gennes conjectures," Phys. Rev. E **92**, 020301 (2015).

[38] Gallier, S., Simulation numérique de suspensions frictionnelles. Application aux propergols solides, Ph.D. thesis, Université Nice Sophia Antipolis, 2014.

[39] Zhang, S., L. Zhang, M. Bouzid, D. Z. Rocklin, E. Del Gado, and X. Mao, "Correlated rigidity percolation and colloidal gels," Phys. Rev. Lett. **123**, 058001 (2019).

[40] Yang, M., L. E. Scriven, and C. W. Macosko, "Some rheological measurements on magnetic iron oxide suspensions in silicone oil," J. Rheol. **30**, 1015–1029 (1986).

[41] Corte, L., P. M. Chaikin, J. P. Gollub, and D. J. Pine, "Random organization in periodically driven systems," Nat. Phys. **4**, 420–424 (2008).

[42] Ness, C., R. Mari, and M. E. Cates, "Shaken and stirred: Random organization reduces viscosity and dissipation in granular suspensions," Sci. Adv. **4**, eaar3296 (2018).

[43] Baker, J., and A. Kudrolli, "Maximum and minimum stable random packings of platonic solids," Phys. Rev. E **82**, 061304 (2010).

[44] Lin, N. Y. C., B. M. Guy, M. Hermes, C. Ness, J. Sun, W. C. K. Poon, and I. Cohen, "Hydrodynamic and contact contributions to continuous shear thickening in colloidal suspensions," Phys. Rev. Lett. **115**, 228304 (2015).

[45] Peters, F., G. Ghigliotti, S. Gallier, F. Blanc, and E. L. Lobry, "Rheology of non-Brownian suspensions of rough frictional particles under shear reversal: A numerical study," J. Rheol. **60**, 715–732 (2016).

[46] Divoux, T., C. Barentin, and S. Manneville, "Stress overshoot in a simple yield stress fluid: An extensive study combining rheology and velocimetry," Soft Matter **7**, 9335–9349 (2011).

[47] Cates, M. E., J. P. Wittmer, J.-P. Bouchaud, and P. Claudin, "Jamming, force chains, and fragile matter," Phys. Rev. Lett. **81**, 1841–1844 (1998).

[48] Seto, R., A. Singh, B. Chakraborty, M. M. Denn, and J. F. Morris, "Shear jamming and fragility in dense suspensions," Granul. Matter **21**, 82 (2019).

[49] Morris, J. F., "Shear thickening of concentrated suspensions: Recent developments and relation to other phenomena," Annu. Rev. Fluid Mech. **52**, 121–144 (2020).